J Geophys (1983) 52:22–33

Inductive Coupling Between Idealized Conductors and Its Significance for the Geomagnetic Coast Effect

Detlef Wolf
Department of Physics, University of Toronto, Toronto, Ontario, Canada, M5S 1A7

Abstract. A problem of current interest is the inductive coupling between an ocean, a solid earth conductor and a conductosphere. The anomaly of this configuration is modelled by (i) the inductive response of a system consisting of two thin half planes and an underlying thin whole plane and (ii) the superposition of the responses of two related systems, each consisting of only one of the two half plane and the whole plane. The configuration is two-dimensional, and the planes are perfectly conducting. These two assumptions allow the derivation of rigorous solutions for the induced magnetic fields by conformal mapping methods. A comparison between the anomalies (i) and (ii) permits the determination of the degree of inductive coupling between the idealized conductors. This establishes a reference for estimating the inductive coupling between more realistic conductors and may therefore assist in the interpretation of complicated magnetic variation anomalies in coastal regions. Our substitute configurations can also be used directly for the rapid modelling of the inductive response of the earth in the vicinity of coastlines. This is demonstrated by analyzing some field data from the recent literature.

Key words: Electromagnetic induction — Inductive coupling — Geomagnetic coast effect — Conformal mapping

Introduction

The behaviour of the geomagnetic variation vector in the vicinity of coastlines is characterized by the fact that it is closely confined to a certain plane, which has been called the preferred plane. This plane often strikes approximately parallel to the continental margin, and its orientation is nearly independent of the polarization and frequency characteristics of the inducing field. The whole phenomenon has been coined the geomagnetic coast effect and was first described by Parkinson (1959). Clearly, this effect is related to the sharp conductivity contrast between sea-water and adjacent rocks. However, there is evidence for the interference by other conductivity anomalies in coastal regions. These have sometimes been correlated with temperature anomalies in the upper mantle along recent subduction zones due to a cold, descending lithospheric slab or partial melting (Schmucker et al., 1966; Greenhouse et al., 1973; Honkura, 1978). In other cases they are believed to be signatures of mineralogical or petrological changes in the lower crust, such as hydrous minerals or ancient plate boundaries (Hyndman and Hyndman, 1968; Edwards and Greenhouse, 1975).

The exact determination of the inductive response of a real (three-dimensional) ocean is a difficult task. Reliable solutions may be obtained from scale model experiments (Dosso, 1973). Alternatively, analytical or numerical solutions can be used, such as for three-dimensional induction in a thin layer of finite conductivity, overlying a homogeneous or layered half space (Vasseur and Weidelt, 1977; Dawson and Weaver, 1979). This raises the question as to how to "deduct" the response of the model ocean from the actually observed coastal anomaly in a realistic manner. Such a reduction is necessary, if an interpretation of the observed anomaly in terms of the conductivity structure of the lower crust or upper mantle alone is required. An obvious way to allow for the influence of the ocean is to subtract its anomaly. But this simple procedure neglects any inductive coupling existing even between insulated conductors, which may be significant. This has already been emphasized by Price (1964) and Rikitake (1966).

To shed some light on this problem, two deliberately simple classes of models (in the following denoted as cases A and B), which are nevertheless characteristic for actual conductivity structures near coastlines, are considered here. They involve only perfectly conducting half and whole planes of two-dimensional configuration. It is shown that the extent of inductive coupling is different for the two cases, which leads us to distinguish between what we call an additive case A and a coupled case B. These ideal configurations can serve as useful standards, as they establish an upper limit on the inductive coupling to be expected for more realistic models.

Application of Conformal Mapping to Electromagnetic Induction

Conformal mapping methods have been applied to problems of geomagnetic induction by Schmucker (1964; 1970a), Greenhouse et al. (1973), Weidelt (1981)

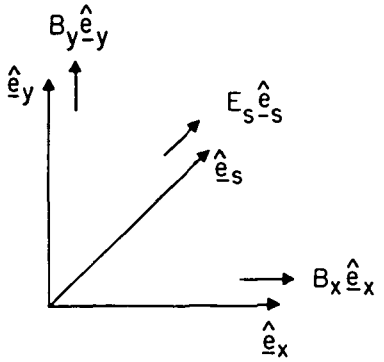

Fig. 1. Co-ordinate system used: s designates the direction tangential to strike, whereas x and y designate the horizontal and vertical directions, respectively, in a plane normal to strike (also see text)

and others. The mathematical principles are given in Morse and Feshbach (1953) and Koppenfels and Stallmann (1959). For our purposes, we adopt the following assumptions.

(i) The geometry of the induction problem is two-dimensional, i.e. an arbitrary function f of the Cartesian space co-ordinates, can be written as $f=f(x,y)$ (Fig. 1).

(ii) The E polarization case applies (Fig. 1).

(iii) The conductors are perfect, and the non-conducting region of the (x,y) plane is a simply connected domain.

Since the interior of the perfect conductors is assumed to be source-free, the boundary conditions at any interfaces between perfectly conducting and non-conducting regions are

$$\hat{\mathbf{e}}_n \cdot \mathbf{B} = 0, \tag{1}$$

$$\hat{\mathbf{e}}_n \times \mathbf{H} = \mathbf{K}, \tag{2}$$

where $\mathbf{K}$ is the surface current density and $\mathbf{H}$ the magnetic field, with $\mathbf{B}=\mu_0\mathbf{H}$ as the magnetic induction. $\hat{\mathbf{e}}_n$ designates the unit vector normal to the interface. As displacement currents are neglected, we can write the magnetic induction in terms of a vector or scalar potential, respectively

$$\mathbf{B} = \nabla \times \psi, \tag{3}$$

$$\mathbf{B} = \nabla \phi. \tag{4}$$

But since we consider E polarization, we have $\psi = \psi \hat{\mathbf{e}}_s$. Here $\hat{\mathbf{e}}_s$ denotes the unit vector in the strike direction (Fig. 1). $\psi = |\psi|$ is a magnetic stream function. Considering the component forms of Eqs. (3) and (4), it can also be shown that $\phi(x,y)$ and $\psi(x,y)$ satisfy the Cauchy-Riemann conditions and are therefore harmonic functions. As this opens the possibility of using conformal mapping methods, we introduce complex quantities and define an analytical magnetic potential by

$$\Omega(z) = \Omega(x+iy) = \phi(x,y) + i\psi(x,y). \tag{5}$$

But as $d\Omega/dz = \partial\phi/\partial x + i\partial\psi/\partial x$, the analytic magnetic field is then given by

$$B(z) = B(x+iy) = B_x(x,y) - iB_y(x,y), \tag{6}$$

where the component forms of Eqs. (3) and (4) have been used. The concept of solving two-dimensional boundary-value problems of potential theory by conformal mapping can now be stated as follows. As a start, a trivial boundary-value problem is formulated in a complex auxiliary plane, the w plane. This auxiliary plane is then "deformed" as necessary, such that the solution of the actual boundary-value problem in the complex z plane is obtained. Mathematically, this transformation is represented by a conformal mapping $w(z)$, where $w=u+iv$ and $z=x+iy$. If $\Omega(w)$ is the solution for the potential in the w plane, the required solution in the z plane can then be written as $\Omega(z) = \Omega(w(z))$, where $w(z)$ must be known. That $\Omega(z)$ in fact constitutes the solution for the actual boundary-value problem can be proven if the mathematical properties of the functions $\Omega(w)$ and $w(z)$ are exploited.

Solutions for some Perfectly Conducting Thin Sheet Configurations

Significance of Perfect Conductors

In this section, some induction problems are formulated in terms of perfectly conducting half and whole planes in a non-conducting environment. In view of the conductivity distribution of the real earth, this is obviously a highly idealized model. However, there are important facts that justify this choice.

For electromagnetic induction phenomena, a distribution of perfectly conducting and non-conducting regions constitutes the inductive limit, i.e. inductive effects completely dominate resistive effects. Since we are going to estimate the degree of electromagnetic interaction between galvanically insulated conductors, a distribution of perfect conductors is a useful limit to consider.

On the other hand, a particular geophysical interpretation can be attached to our induction problem. It is the situation in which a laterally discontinuous solid earth conductor is adjacent to an ocean and both are underlain by a highly conducting region at some depth. Even though there is evidence for such situations in several coastal regions (e.g. Bailey et al., 1974; Edwards and Greenhouse, 1975), no systematic investigation of the electromagnetic interaction between such conductors has been attempted so far. Lines et al. (1973) solved a related problem numerically, but the emphasis was on the detectability of an anomalous upper mantle beneath an ocean. Their formulation of the coupling problem was not rigorous, and only a special and complicated model was examined. For investigating inductive coupling, simple but versatile combinations of thin sheets are more promising, because the number of free parameters remains small. If only the inductive limit is considered, we thus have distributions of perfectly conducting half and whole planes, which are discussed here.

However, the representation of real conductors by ideal models of this kind has some notable implications. If, for example, a perfectly conducting half plane is considered, the conductor it replaces must be thick relative to its own skin depth, but also thin relative to the skin depth of its host. According to Bailey

(1977), for oceans and earth conductors of a regional scale, there is no frequency such that this condition applies strictly. On the other hand, if we confine ourselves to the interpretation of the in-phase part of the observed response, we are led to the concept of perfect substitute conductors. The general relation between a distribution of perfect substitute conductors and the corresponding imperfect conductivity distribution of the real earth cannot be expressed in simple terms. But considering results obtained for a layered earth (Schmucker, 1970b; Weidelt, 1972), the top interface of a perfectly conducting substitute region ought to mark approximately the mean depth of the induced in-phase currents in the real earth.

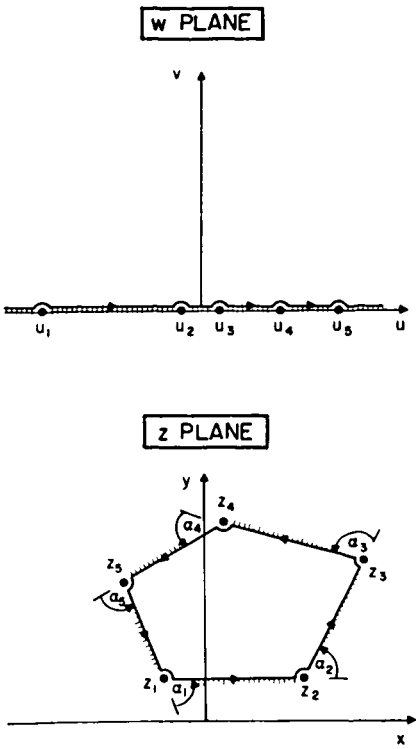

Fig. 2. Schwarz-Christoffel transformation (also see text)

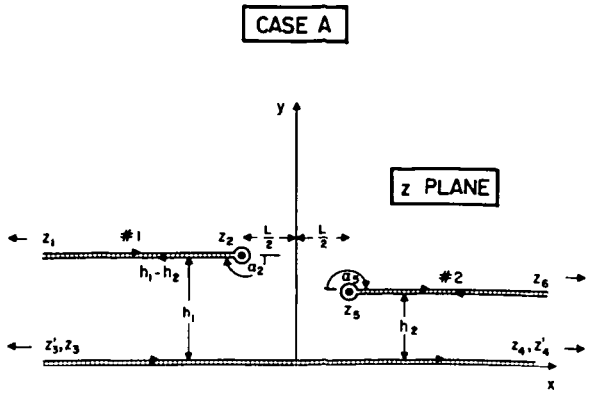

Fig. 3. Conductor configurations (degenerate polygons) for case A. Three distinct combinations of one or two conducting half planes and one conducting whole plane are possible (conductors are hatched): Model A.L.1: Half plane 1 ($x<-L/2$, $y=h_1$) and whole plane ($y=0$). Model A.R.2: Half plane 2 ($x>+L/2$, $y=h_2$) and whole plane ($y=0$). Model A.L.1/R.2: Half plane 1 ($x<-L/2$, $y=h_1$), half plane 2 ($x>+L/2$, $y=h_2$) and whole plane ($y=0$)

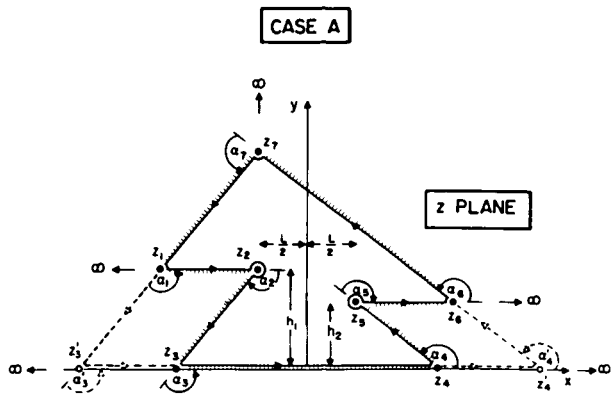

Fig. 4. Ordinary polygons corresponding to the three degenerate cases of Fig. 3. Three distinct polygons are shown: Model A.L.1: Vertices at z_1, z_2, z_3, z'_4, z_7. Model A.R.2: Vertices at z'_3, z_4, z_5, z_6, z_7. Model A.L.1/R.2: Vertices at z_1, z_2, z_3, z_4, z_5, z_6, z_7

Construction of Conformal Mappings

We consider some elementary two-dimensional configurations which involve only parallel and perfectly conducting half and whole planes. To derive the solutions for these configurations, conformal mapping theory is applied using the Schwarz-Christoffel transformation. An alternative approach based on the Cauchy integral formula has been outlined by Wolf (1982a).

The Schwarz-Christoffel transformation (Morse and Feshbach, 1953; Koppenfels and Stallmann, 1959) describes the mapping of the upper half of the w plane onto the interior of an arbitrary polygon of the z plane. Figure 2 illustrates the situation for a polygon with five vertices. In general we have $z_\mu = z(u_\mu)$, where $\mu = 1, \ldots, m$, for the co-ordinates of the vertices.

Here the surfaces of all (two-dimensional) conductors are assumed to coincide with the contours of integration in the w or z planes (see the hatching in Figs. 2–6, especially the cross-sections of perfectly conducting half and whole planes in Figs. 3 and 5). In particular, we consider two basic cases, which are designated as case A (Figs. 3 and 4) and case B (Figs. 5 and 6). In this section, the transformation formulae $z(w)$ for the different models included in cases A and B are summarized. The origin and orientation of the co-ordinate system adopted is evident from Figs. 3–6, which also show the meaning of the geometrical parameters h_1, h_2 and L appearing in the formulae. More details on the mathematical aspects can be found in Wolf (1982a).

Case A comprises the models of three distinct polygons, certain parts of which are congruent. If the vertices approach infinity as indicated in Fig. 4, three corresponding degenerate polygons (combinations of half and whole planes) result (Fig. 3).

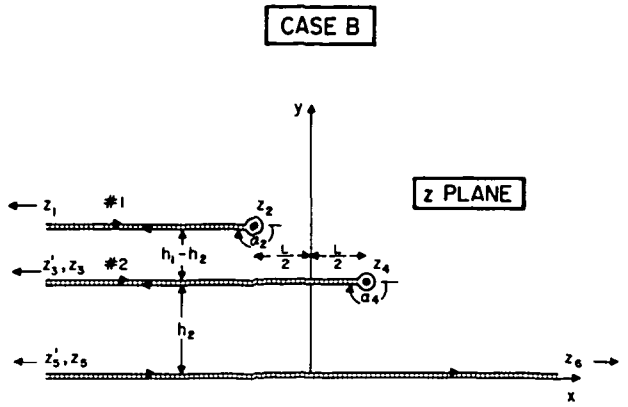

Fig. 5. Conductor configurations (degenerate polygons) for case B. Three distinct combinations of one or two conducting half planes and one conducting whole plane are possible (conductors are hatched): Model B.L.1: Half plane 1 ($x < -L/2$, $y = h_1$) and whole plane ($y = 0$). Model B.L.2: Half plane 2 ($x < +L/2$, $y = h_2$) and whole plane ($y = 0$). Model B.L.1/L.2: Half plane 1 ($x < -L/2$, $y = h_1$), half plane 2 ($x < +L/2$, $y = h_2$) and whole plane ($y = 0$)

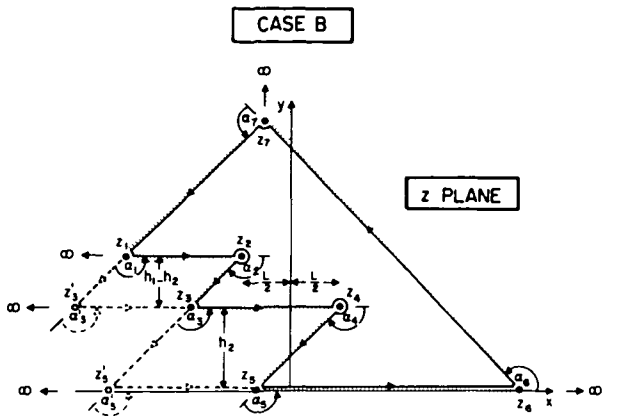

Fig. 6. Ordinary polygons corresponding to the three degenerate cases of Fig. 5. Three distinct polygons are shown: Model B.L.1: Vertices at z_1, z_2, z_5', z_6, z_7. Model B.L.2: Vertices at z_3', z_4, z_5, z_6, z_7. Model B.L.1/L.2: Vertices at z_1, z_2, z_3, z_4, z_5, z_6, z_7

Model A.L.1: Half plane 1 has its edge at $z_2 = -L/2 + ih_1$ and extends towards $x = -\infty$ (L="left"). The whole plane is at $y = 0$. The transformation formula is

$$z(w) = w + a + \frac{h_1}{\pi}\left[\ln(w+a) - \ln\frac{h_1}{\pi} + 1\right] - \frac{L}{2}. \tag{7}$$

Parameter a is defined by $z_3 = z(u_3) = z(-a)$, where u_3 is arbitrary. This model has been considered by Schmucker (1970a) in his attempt to explain the Californian coastal anomaly.

Model A.R.2: Half plane 2 has its edge at $z_5 = +L/2 + ih_2$ and extends towards $x = +\infty$ (R="right"). The whole plane is at $y = 0$. The transformation formula is

$$z(w) = w - a - \frac{h_2}{\pi}\left[\ln(w-a) - \ln\frac{h_2}{\pi} + 1 - i\pi\right] + \frac{L}{2}. \tag{8}$$

Parameter a is defined by $z_4 = z(u_4) = z(a)$, and u_4 may be chosen at will.

Model A.L.1/R.2: Half planes 1 and 2 and the whole plane are located as before. Now we have the transformation

$$z(w) = w + \frac{h_1}{\pi}\ln\frac{w+a}{\sqrt{2h_1 a/\pi}} - \frac{h_2}{\pi}\ln\frac{w-a}{\sqrt{2h_2 a/\pi}} + \frac{h_1 - h_2}{2\pi} + ih_2. \tag{9}$$

Here parameter a is not arbitrary but implicitly given by

$$L = 2\sqrt{k_1} + \frac{h_1}{\pi}\ln\frac{\left[\sqrt{k_1} + \left(a - \frac{h_1 - h_2}{2\pi}\right)\right]^2}{2h_1 a/\pi} + \frac{h_2}{\pi}\ln\frac{\left[\sqrt{k_1} + \left(a + \frac{h_1 - h_2}{2\pi}\right)\right]^2}{2h_2 a/\pi}, \tag{10}$$

where $k_1 \equiv \frac{(h_1 - h_2)^2}{4\pi^2} + \frac{(h_1 + h_2)a}{\pi} + a^2$. It is related to u_3 and u_4 by $z_3 = z(u_3) = z(-a)$ and $z_4 = z(u_4) = z(a)$. The special symmetrical configuration $h_1 = h_2$ of this model has already been discussed by Schmucker (1964, 1970a) with reference to the anomaly caused by a (two-dimensional) island structure. The responses of models A.L.1 and A.R.2 can be superimposed and compared with the response of model A.L.1/R.2.

Case B also consists of three distinct polygons, certain parts of which are congruent. Referring to Figs. 5 and 6, we distinguish the following models.

Model B.L.1: Half plane 1 has its edge at $z = -L/2 + ih_1$ and extends towards $x = -\infty$ (L="left"). The whole plane is at $y = 0$. This model is identical with model A.L.1 and Eq. (7) represents the proper transformation. But now parameter a is defined by $z_5' = z(u_5') = z(-a)$, where u_5' is arbitrary.

Model B.L.2: Half plane 2 has its edge at $z_4 = +L/2 + ih_2$ and extends towards $x = -\infty$ (L="left"). The whole plane is at $y = 0$. This model is closely related to models A.L.1 and B.L.1. The transformation formula is

$$z(w) = w - a + \frac{h_2}{\pi}\left[\ln(w-a) - \ln\frac{h_2}{\pi} + 1\right] + \frac{L}{2}. \tag{11}$$

Parameter a is again arbitrary and related to u_5 by $z_5 = z(u_5) = z(a)$.

Model B.L.1/L.2: Half planes 1 and 2 and the whole plane are located as before. We have the transformation formula

$$z(w) = w + \frac{h_1 - h_2}{\pi}\ln\frac{w+a}{\sqrt{2(h_1 - h_2)a/\pi}} + \frac{h_2}{\pi}\ln\frac{w-a}{\sqrt{2h_2 a/\pi}} + \frac{h_1}{2\pi} \tag{12}$$

Parameter a is not arbitrary but given by

$$L=2\sqrt{k_2}+\frac{h_1-h_2}{\pi}\ln\frac{\left[\sqrt{k_2}+\left(a-\frac{h_1}{2\pi}\right)\right]^2}{2(h_1-h_2)\,a/\pi}$$
$$-\frac{h_2}{\pi}\ln\frac{\left[\sqrt{k_2}+\left(a+\frac{h_1}{2\pi}\right)\right]^2}{2h_2\,a/\pi} \tag{13}$$

with $k_2\equiv\frac{[h_2+(h_1-h_2)]^2}{4\pi^2}-\frac{[h_2-(h_1-h_2)]\,a}{\pi}+a^2$. The interrelation between a, u_3 and u_5 is evident from a consideration of $z_3=z(u_3)=z(-a)$ and $z_5=z(u_5)=z(a)$. Eqs. (7), (11) and (12) allow us again to compare the sum of the responses of models B.L.1 and B.L.2 with the response of model B.L.1/L.2.

Inversions of Mappings and Solutions for Magnetic Potential

As was emphasized above, the problem of obtaining solutions for the models of cases A and B reduces to deriving the solutions $\Omega(w)$ for the boundary-value problem in the w plane and obtain the transformations $w(z)$. The corresponding inverse functions $z(w)$ for the various models have been presented above. Thus, if $\Omega(w)$ is known, it remains to calculate $w(z)$ from $z(w)$.

In the w plane we assumed a perfectly conducting whole plane at $v=0$ (see Fig. 2). A simple solution for this configuration is a potential that yields a homogeneous magnetic field of unit strength in the u direction. Thus

$$\Omega(w)=w, \tag{14}$$

$$B(w)=1. \tag{15}$$

Transformation to the z plane yields

$$\Omega(z)=w(z), \tag{16}$$

$$B(z)=\frac{dw}{dz}. \tag{17}$$

If we consider the different mappings $z(w)$, we realize that, for $z\to\infty$, we again have a homogeneous and horizontal field of unit strength. Our different conductor configurations in the z plane are therefore subject to a uniform inducing field. This is the magnetic source field most widely assumed. A discussion of the limitations of this assumption has been given by several authors, e.g. Price (1964).

However, to obtain solutions $\Omega(z)$ or $B(z)$ at any point in the z plane, our solutions $z(w)$ must be inverted numerically. Here we have used the Newton-Raphson iteration scheme. This algorithm has also been employed to calculate parameter a by inverting Eqs. (10) and (13). With $w(z)$ thus determined, we can then calculate $\Omega(z)$ and $B(z)$ according to Eqs. (16) and (17). But due to Eqs. (5) and (6), the quantities ϕ, ψ, B_x, B_y are also determined, and we can consider various transfer functions as necessary.

Inductive Coupling Between Ocean, Earth Conductor and Conductosphere

General Remarks

Now we present some results for the models described above. To facilitate our discussion, a common normalization of the magnetic field components is adopted. We define as normal the field at a point far away from the lateral discontinuity, where the conductivity structure is effectively one-dimensional.

The following decompositions of the total field components can then be performed (Schmucker, 1964; 1970a).

$$B_x=B_{xn}+B_{xa}, \tag{18}$$

$$B_y=B_{yn}+B_{ya}. \tag{19}$$

Here $B_{yn}=0$, because the source fields are uniform. Due to the linearity of the Maxwell equations and in the limit of perfect conductivity we can then write in terms of two quantities, S_{xx} and S_{yx},

$$B_{xa}(t)=S_{xx}B_{xn}(t), \tag{20}$$

$$B_{ya}(t)=S_{yx}B_{xn}(t). \tag{21}$$

S_{xx} and S_{yx} are the (real) horizontal and vertical Schmucker transfer functions, respectively. Other response parameters, such as the Parkinson transfer function, i.e. B_y/B_x, could also be used. But for our purposes, the Schmucker transfer functions are more useful, as their common normalization gives a true representation of the degree of the inductive coupling. The interrelation between several real transfer functions (induction vectors) has recently been discussed by Wolf (1982b).

All lengths are normalized relative to the separation h_1 between half plane 1 and the whole plane, and the inductive response for several values of the ratios h_2/h_1 and L/h_1 is investigated. However, to gain some basic insight first, the normalized field distribution for two characteristic configurations of models A.L.1/R.2 and B.L.1/L.2 are shown in Figs. 7 and 8, respectively. The forcing of the field vectors about the edges of the half planes is very conspicuous. This behaviour is related to the fact that the magnetic field must be tangential to the surfaces of the perfect conductors. The screening effect of the half planes is also displayed, but some magnetic flux "leaks" into the region between the half planes and the whole plane.

When interpreting our results below, emphasis is placed on the inductive coupling between the conductors. More specifically, we compare the sum of the responses of two models, each one involving only one half plane parallel to a whole plane, with the response of the corresponding complete model consisting of both half planes and the whole plane. Theoretically, the latter response is not identical to the sum of the two individual responses, because of a redistribution of the current systems in all three conductors due to their interaction.

To give our results some geophysical relevance, we let half plane 1 represent an ocean and half plane 2 a laterally discontinuous earth conductor. The underlying whole plane is associated with the conductorsphere, i.e.

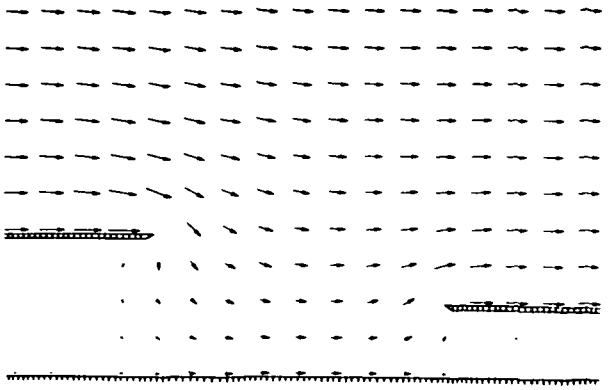

Fig. 7. Distribution of magnetic field vectors for model A.L.1/R.2 ($L/h_1 = 2.0$, $h_2/h_1 = 0.5$). No vector has been plotted at the edge of the sheet, where the field is singular

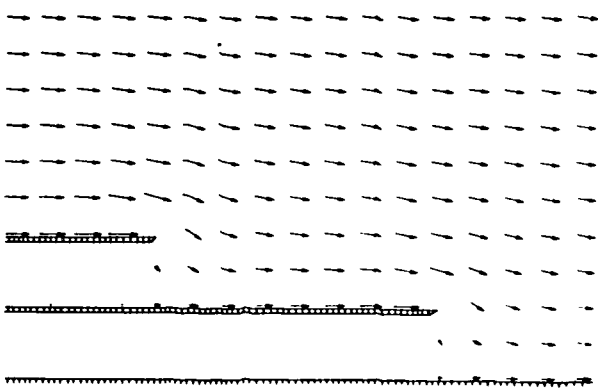

Fig. 8. Distribution of magnetic field vectors for model B.L.1/L.2 ($L/h_1 = 2.0$, $h_2/h_1 = 0.5$). No vector has been plotted at the edge of the sheet, where the field is singular

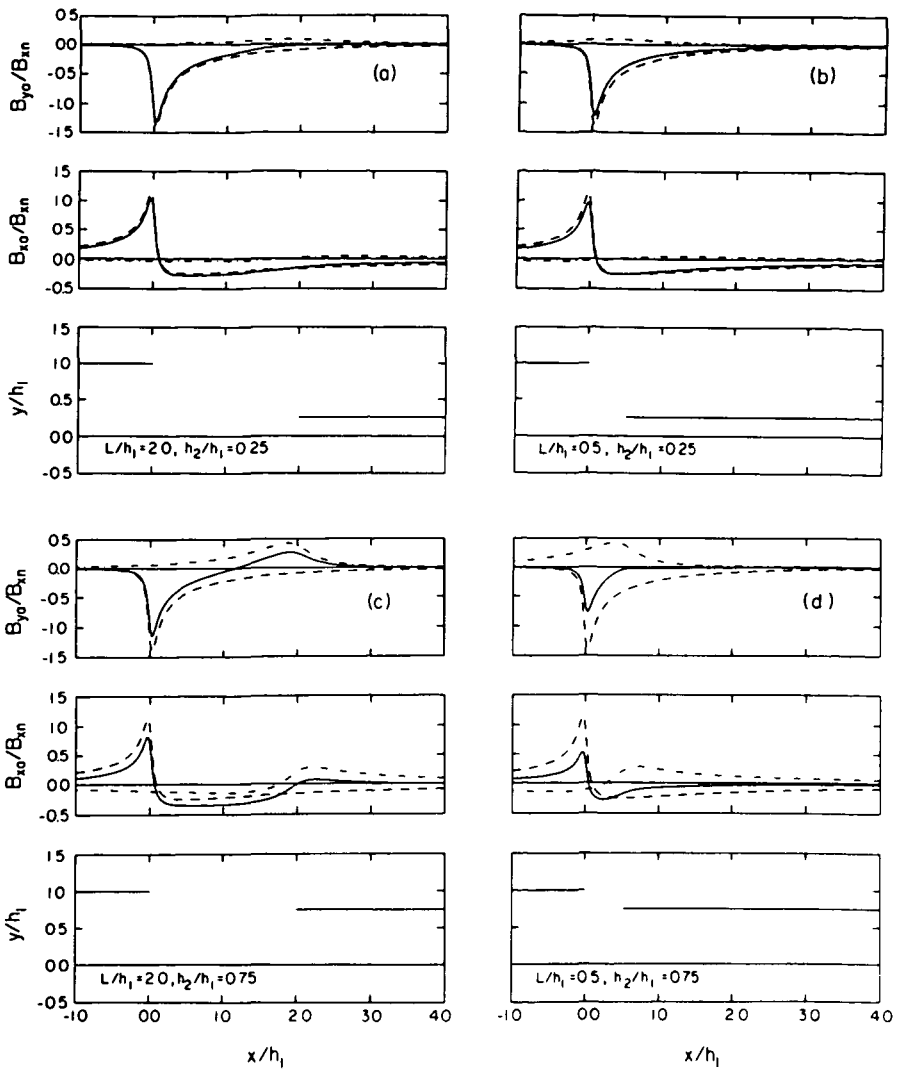

Figs. 9a–d. *Top* Schmucker vertical transfer functions for model A.L.1 (dashed), model A.R.2 (dot-dashed) and model A.L.1/R.2 (solid) *Center* As top but for Schmucker horizontal transfer functions *Bottom* Corresponding conductor configurations (solid) and position of measuring profile (dotted) For further explanations see text

with the depth range of the sharp downward increase of conductivity, for the particular frequency being considered. We have calculated the Schmucker transfer functions along a horizontal profile close to the level of the ocean. The separation h_3 between this profile and the conductosphere has always been chosen to be 105% of the separation h_1 between the ocean and the conductosphere ($h_3/h_1 = 1.05$). Although this choice may appear arbitrary, it takes into account the fact that the centre of the (in-phase) current distribution must be

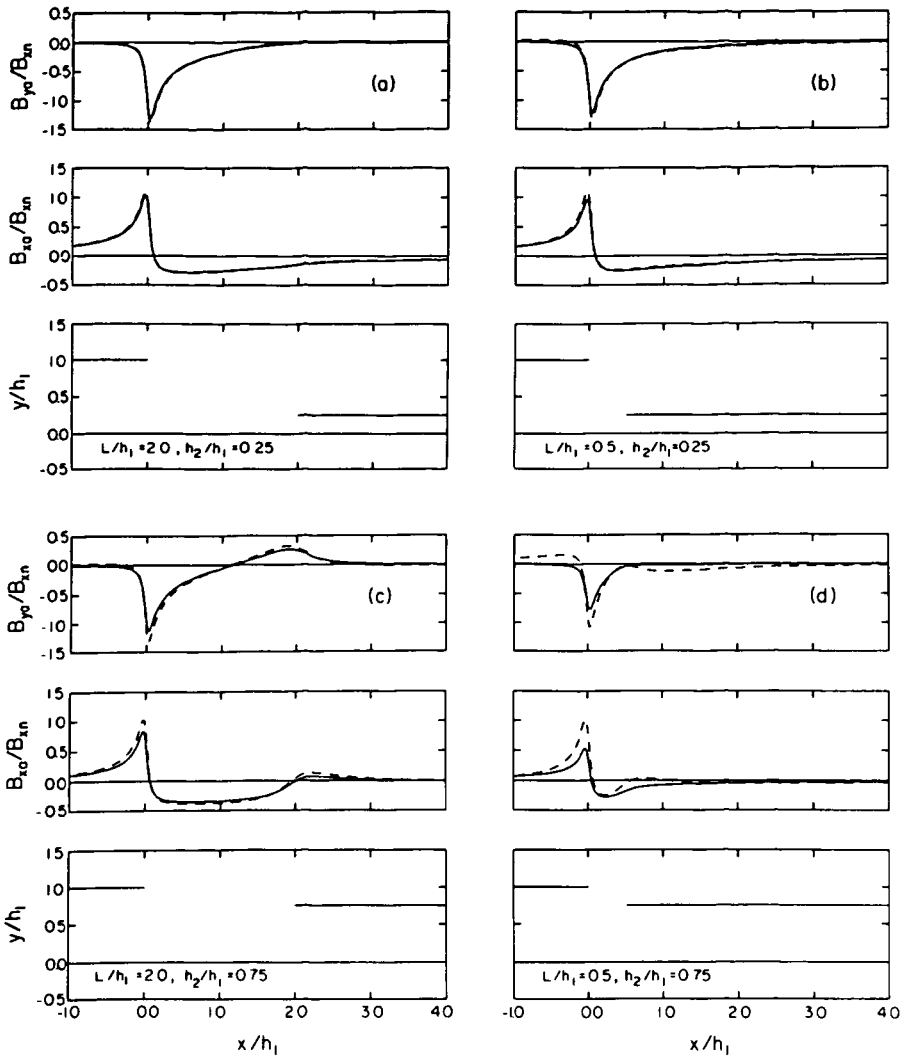

Figs. 10a–d. *Top:* Sum of Schmucker vertical transfer functions for models A.L.1 and A.R.2 (dashed) and Schmucker vertical transfer function for model A.L.1/R.2 (solid). *Center:* As top but for Schmucker horizontal transfer functions. *Bottom:* Corresponding conductor configurations (solid) and position of measuring profile (dotted). For further explanations see text

below the surface of a real ocean and no singularities are observed along ocean-continent boundaries.

Case A: Numerical Results and Discussion

The configurations considered belong to models A.L.1, A.R.2 or A.L.1/R.2. Here the perturbation of the edge anomaly of a laterally discontinuous earth conductor (model A.R.2) by an adjacent ocean (model A.L.1) is of most interest to us. A different interpretation would be to consider the perturbation of the "ordinary" ocean anomaly (model A.L.1) by including an earth conductor (model A.R.2) at some distance from the coast. In either case, the resulting response (model A.L.1/R.2) is a combination of the effects of both the linear superposition of the individual current systems and their redistribution due to their mutual interaction.

The responses of many conductor configurations have been calculated during these investigations. However, a limited number of geometries suffices for a demonstration of the general behaviour, and only combinations of the following ratios are considered: $L/h_1 = 0.5$, 2.0 and $h_2/h_1 = 0.25$, 0.75, which gives a total of four configurations.

Let us first discuss the characteristics of the Schmucker vertical transfer function, i.e. the normalized (anomalous) vertical field. Then the ocean anomaly is negative throughout, whereas the edge anomaly of the earth conductor is always positive (Figs. 9a-d). If linear superposition holds, the magnitude of the latter anomaly therefore decreases by the magnitude of the ocean anomaly. The top panels of Figs. 9a-d allow us to compare the normalized vertical field of the four configurations of model A.L.1/R.2 (solid line) with that of the corresponding four configurations without an ocean (model A.R.2, dot-dashed line). If we focus on the section of the profile above the edge of the earth conductor, we can observe the following. Usually, the vertical field of the complete configuration (solid) approximates the sum of the vertical fields of the two individual configurations very closely, i.e. the edge anomaly of the earth conductor (dot-dashed) is in fact diminished by the magnitude of the anomaly of the ocean (dashed). The response of a deep earth conductor ($h_2/h_1 = 0.25$) close to the edge of the ocean ($L/h_1 = 0.5$) is therefore completely masked by the comparatively strong response of the latter (Fig. 9b). On the other hand, for a shallow earth conductor ($h_2/h_1 = 0.75$) close

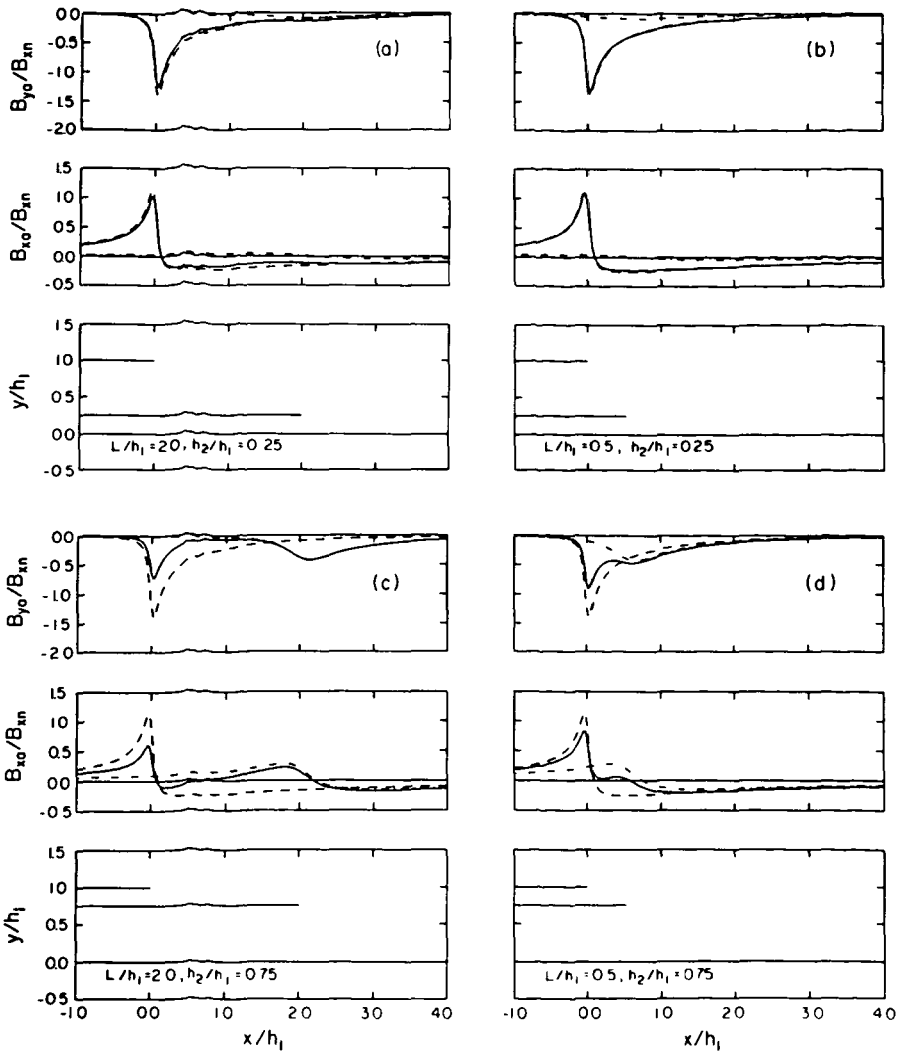

Figs. 11a–d. *Top* Schmucker vertical transfer functions for model B.L.1 (dashed), model B.L.2 (dot-dashed) and model B.L.1 L.2 (solid). *Center* As top but for Schmucker horizontal transfer functions *Bottom* Corresponding conductor configurations (solid) and position of measuring profile (dotted). For further explanations see text

to the edge of the ocean ($L/h_1=0.5$), some electromagnetic interaction can be identified (Fig. 9d). This is not surprising, because the distance between the edges of half planes 1 and 2 is now comparable with or less than either half plane's separation from the conducting whole plane underneath.

We have also calculated the Schmucker horizontal transfer functions, which are equal to normalized anomalous horizontal fields, for the same configurations (Figs. 9a–d, centre panels, respectively). Since the ocean anomaly is negative in the region above the earth conductor, linear superposition causes a downward shift of the edge anomaly of the earth conductor by the magnitude of the ocean anomaly. From the individual figures it is obvious that, for a deep continental conductor ($h_2/h_1=0.25$), additivity of the anomalies holds to a very good approximation (Figs. 9a and b). But again its response is almost completely masked by the comparatively strong response of the ocean. However, if the earth conductor is shallow ($h_2/h_1=0.75$), its edge anomaly becomes very conspicuous (Figs. 9c and d). The anomalous horizontal fields are roughly additive, except when the edges of half planes 1 and 2 are very close ($L/h_1=0.5$).

To distinguish the effect of interaction more clearly, the sum of the magnetic fields according to models A.L.1 and A.R.2 (dashed lines) has been calculated and compared with the magnetic field of model A.L.1 R.2 (solid lines). The results are shown in Figs. 10a–d for the four configurations, for vertical (top panels) and horizontal transfer functions (centre panels). The nearly complete additivity of the anomalies for a deep earth conductor ($h_2/h_1=0.25$) is corroborated by Figs. 10a and b. But, if it is shallow ($h_2/h_1=0.75$), some inductive coupling can be identified. It mainly causes an attenuation of the peak values of the anomalies, as compared with the corresponding peaks of the superimposed anomalies (Figs. 10c and d).

Case B. Numerical Results and Discussion

Now the configurations are those of models B.L.1, B.L.2 or B.L.1 L.2. The earth conductor (half plane 2) extends from below the ocean (half plane 1) towards the land. In interpreting the following model curves, we again concentrate on the perturbation of the inductive response of a laterally discontinuous earth conductor (model B.L.2) by an ocean (model B.L.1), which leads

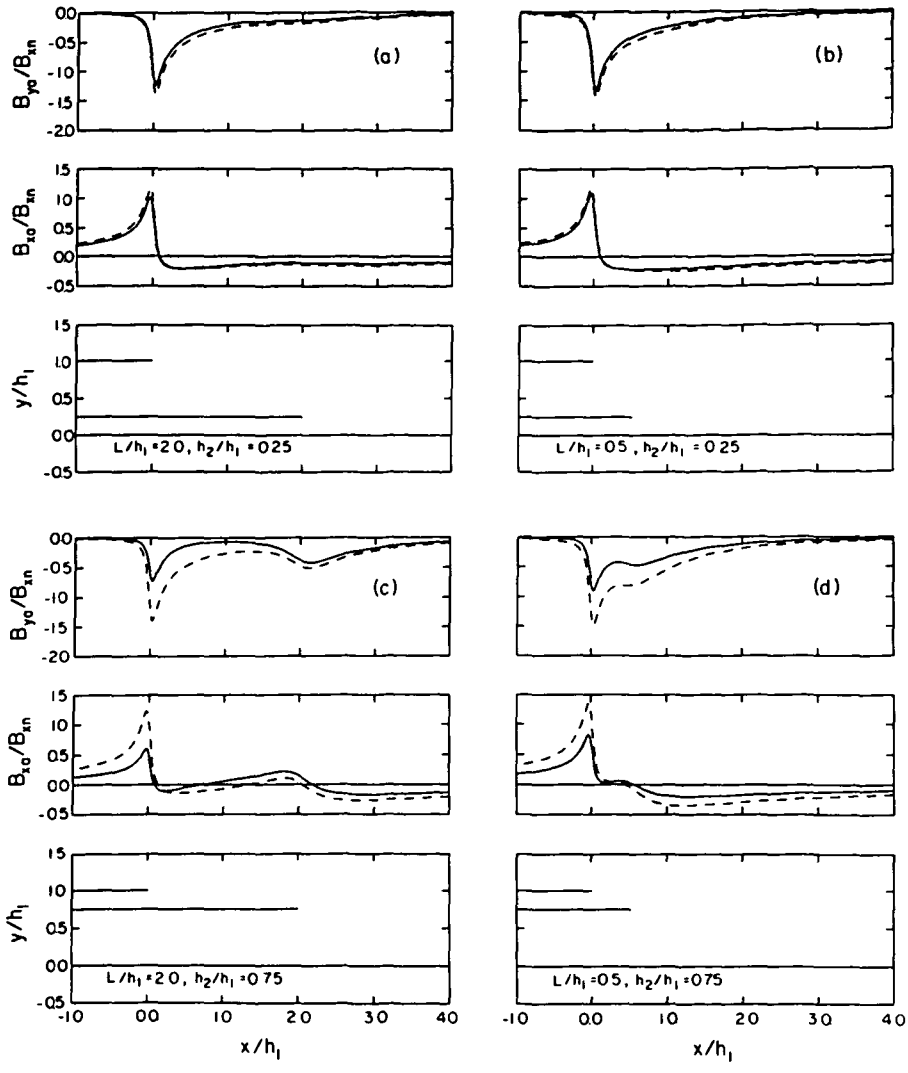

Figs. 12a-d. *Top:* Sum of Schmucker vertical transfer functions for models B.L.1 and B.L.2 (dashed) and Schmucker vertical transfer function for model B.L.1/L.2 (solid). *Center:* As top but for Schmucker horizontal transfer functions. *Bottom:* Corresponding conductor configurations (solid) and position of measuring profile (dotted). For further explanations see text

to the complete model B.L.1/L.2. A different interpretation is, as before, to consider the perturbation of the undisturbed ocean response (model B.L.1) by an additional earth conductor (model B.L.2). This causes an attenuation of the ocean response due to the decrease of the ocean's separation from the coupling surface below. Our discussion is again limited to configurations with the following geometrical parameters: $L/h_1 = 0.5$, 2.0 and $h_2/h_1 = 0.25$, 0.75, which yields a total of four configurations.

Normalized vertical fields are presented in the top panels of Figs. 11a-d, respectively. When interpreting the individual figures, the following points should be borne in mind. Both ocean and earth conductor cause negative vertical fields. Thus, for linear superposition, the magnitude of the edge anomaly of the earth conductor increases by the magnitude of the ocean anomaly. We may, near the edge of the earth conductor, compare the complete response (model B.L.1/L.2, solid line) with the response of the corresponding configuration without an ocean (model B.L.2, dot-dashed line). Then we realize that linear superposition does not hold as accurately as for case A, particularly if the earth conductor is shallow ($h_2/h_1 = 0.75$). Here, its "pure" edge anomaly according to model B.L.2 remains virtually unchanged after the ocean has been included in the solution (model B.L.1/L.2). This is to be expected, because the inductive coupling between half plane 1 and the whole plane corresponding to model B.L.1 has now been replaced by the stronger coupling between half planes 1 and 2. This in turn leads to a pronounced attenuation of the anomaly associated with the ocean, such that it has almost faded away near the edge of the earth conductor (see particularly Fig. 11c). If the edges of half planes 1 and 2 are very close ($L/h_1 = 0.5$), additional interactions arise between them (Fig. 11d).

The Schmucker horizontal transfer functions are displayed in the centre panels of Figs. 11a-d, respectively. If linear superposition holds, the ocean anomaly causes a downward shift of the edge anomaly of the earth conductor by the magnitude of the ocean anomaly. The calculated shift (solid line) is always less, and a closer inspection of Figs. 11c-d again shows that for shallow earth conductors ($h_2/h_1 = 0.75$) the anomaly due to the ocean must be strongly attenuated. Deep conductors ($h_2/h_1 = 0.25$) are difficult to detect also on

the basis of their associated horizontal transfer functions, but linear superposition now becomes a better approximation (Figs. 11a and b).

These conclusions are also supported by Figs. 12a–d, which compare the sum of the magnetic fields of models B.L.1 and B.L.2 with the magnetic field of model B.L.1/L.2.

Rapid Modelling of Geomagnetic Coast Effects

The solutions presented above have primarily been derived to investigate the degree of inductive coupling between two conducting half planes and an underlying whole plane. However, they may also be used for the direct modelling of measured magnetic variations, as long as the observed response is close to the inductive limit. More general modelling techniques do exist, but the following two examples demonstrate that simple configurations consisting of two half planes and a whole plane often suffice for a representation of the fundamental character of the subsurface conductivity structure. As only three model parameters are involved, trial and error modelling is very rapid, and the final configuration can serve as a useful guide when considering more complicated models of the subsurface conductivity distribution.

Coast Effect in South-Western Australia

As one example, real Parkinson transfer functions, as measured by Everett and Hyndman (1967) in south-western Australia, have been analyzed. Strictly speaking, the authors regarded their transfer functions as vectors (Parkinson arrows) and decomposed them into components perpendicular to two straight lines, which served as crude representations of the edges of the continental shelves west and south of the survey area.

Figure 13 shows the modelling results for the observed transfer function components perpendicular to the west coast for one-hour periods, by a specific conductor configuration of model B.L.1/L.2. The edge of half plane 1 has been taken to coincide with the edge of the continental shelf. The exact height of the measuring profile above this half plane is only crucial for the behaviour of the model response very close to the singular edge of this half plane, where our model becomes inappropriate and no field observations exist anyway. The most interesting aspect is that a second half plane is required to reconcile the observed attenuation of the coast effect close to the continental margin with the large depth of the conductosphere for one-hour periods far away from the ocean, as established by Lilley et al. (1981). Whether this second conductor actually extends below the real ocean, cannot be inferred from our results because the model ocean has been assumed opaque for electromagnetic fields.

To explain the subdued vertical variation at their westernmost station, Everett and Hyndman (1967) proposed that the Australian shield might terminate along the Darling fault, which separates the sedimentary Perth basin to the west from the shield area to the east. In our model, the non-shield region is represented by half plane 2 at a depth of 45 km below the surface,

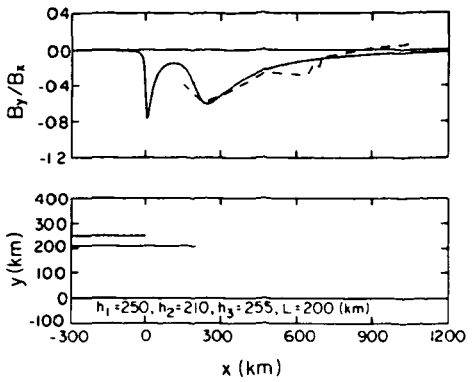

Fig. 13. *Top:* Measured (dashed) and calculated (solid) Parkinson transfer functions as a function of the distance from the continental margin. *Bottom:* Model conductors (solid) and measuring profile (dotted). $T=1$ h, south-western Australia (also see text)

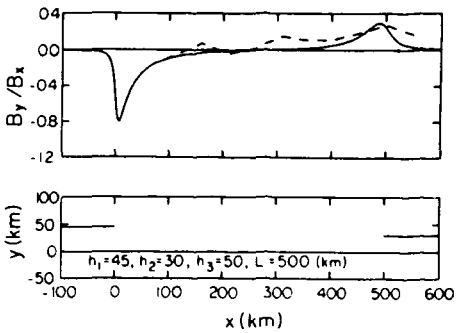

Fig. 14. *Top.* Measured (dashed) and calculated (solid) Parkinson transfer functions as a function of the distance from the continental margin *Bottom:* Model conductors (solid) and measuring profile (dotted). $T=1$ h, eastern United States (also see text)

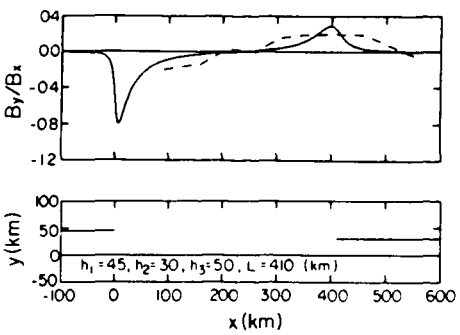

Fig. 15. *Top* Measured (dashed) and calculated (solid) Parkinson transfer functions as a function of the distance from the continental margin. *Bottom* Model conductors (solid) and measuring profile (dotted) $T=16$ min, eastern United States (also see text)

whereas the conductosphere is more than 200 km deep. This is similar to the configuration of Fig. 12d, which has been discussed above.

Coast Effect in the Eastern United States

As a second example, the coast effect observed by Edwards and Greenhouse (1975) in the eastern United

States is considered. In contrast to Everett and Hyndman (1967), the former interpreted the anomalies quantitatively and concluded that a region of enhanced conductivity lay in the lower crust or uppermost mantle at some distance from the ocean. This conductive zone shows an increase in conductivity with increasing distance from the coast.

The general character of their assumed conductivity distribution together with the smallness of the observed out-of-phase response suggest an explanation of the anomaly by model A.L.1/R.2. Since transfer function estimates for the periods of 16 min and 1 h are available, both data sets have been interpreted. Again, the edge of half plane 1 coincides with the edge of the continental shelf. Comparing Fig. 14 (1 h) with Fig. 15 (16 min), their main difference is that, for the shorter period, the earth conductor (half plane 2) extends closer to the ocean, whereas its depth is not affected at all. This is consistent with the model conductor proposed by Edwards and Greenhouse (1975), which has resistivities close to 1 Ωm at some distance from the coast, with a slight rise to about 20 Ωm towards the ocean. In contrast with the Australian results, the conductosphere must now be assumed to begin at a shallow depth. In other words, the lower crust or upper mantle are highly conductive in the eastern United States.

Finer details in the observed response cannot be explained by our simple models. Furthermore, other anomalies may require models that are different. The main aspect to be emphasized here is, however, that our fast modelling technique does have the capability of furnishing basic quantitative information on the conductivity distribution in the ground.

Conclusions and Suggestions for Future Work

It has become obvious that our distinction between cases A and B was not only a matter of mathematical convenience. The conductor configurations corresponding to these two cases also had essentially different response characteristics. This is summarized here.

If we first review the behaviour of model A.L.1/R.2, we realize that its inductive response was almost the sum of the responses of models A.L.1 and A.R.2. This approximation was particularly good if the earth conductor had a large depth ($h_2/h_1 = 0.25$). If it was shallow ($h_2/h_1 = 0.75$), the extent of inductive coupling still remained small and only became more significant for $L/h_1 = 0.50$. We therefore call case A the additive case.

For bodies of finite conductivity, additivity should be a still better approximation, because the relative importance of interaction between conductors decreases with decreasing conductivity. And even if the assumption of a two-dimensional conductivity configuration is violated, the basic behaviour ought to be very similar. A problem of current interest is the interpretation of the combined anomaly of a two-dimensional earth conductor extending away from a three-dimensional ocean. Here the ocean anomaly can simply be subtracted and the residual can be interpreted in terms of the earth conductor alone.

Case B was designed to simulate an earth conductor extending towards the ocean. The corresponding model B.L.1/L.2 incorporates two strongly coupled half planes. Therefore, essentially different response characteristics were to be expected, and the edge effect of the earth conductor was found to be almost unaffected by the ocean. This behaviour was closely followed when the former conductor was shallow ($h_2/h_1 = 0.75$). It was interpreted as being due to the strong attenuation of the response of the ocean caused by its interaction with the earth conductor. Case B is therefore called the coupled case. This emphasizes the fact that the response of the earth conductor at large distances from the ocean was found to be very nearly identical with the anomaly that it causes in close proximity to this ocean.

If bodies of finite conductivity are considered, the interaction between ocean and earth conductor becomes weaker. But it can be expected that the in-phase portion of the earth conductor anomaly still displays this persistency to a high degree. On the other hand, the out-of-phase portion of the ocean anomaly ought not to be attenuated significantly and is probably superimposed on the out-of-phase portion of the anomaly due to the earth conductor.

If the earth conductor of case B was deeper ($h_2/h_1 = 0.25$), its edge effect decreased, whereas the ocean effect increased. The latter was explained by the weaker interaction between both conductors and hence the ocean could not be disregarded. Here the main problem is clearly the separation of the minute signature of the earth conductor from the much stronger ocean anomaly. Any further considerations, such as the question of interaction, are only of minor practical importance by comparison.

We may, however, wish to make explicit allowance for the finite conductivity of the ocean. The numerical method of Greenhouse et al. (1973) appears to be a useful way of doing so. It allows the calculation of the total response of a thin sheet of variable conductivity above a perfectly conducting undulating surface, where the whole configuration is two-dimensional. Various shapes can be assumed for these undulations, e.g. combinations of half planes and steps or elliptical bulges. Also, the response of (i) a finitely conducting sheet above a horizontal conductosphere or (ii) an undulated conductosphere alone, can be calculated separately and then superimposed. This again allows the coupling of the thin sheet and the undulating perfect conductor to be investigated. But, the number of free parameters tends to become larger for such a model. This hinders the task of extracting useful general trends from the results.

Another possible extension of our work is to define a useful inverse problem, which is based on the anomalous response, as observed in the vicinity of a coastline. Weidelt (1981) considered configurations without an ocean and constructed extremal models that maximize the depth below the surface of the top of a perfect conductor. In Weidelt's analysis, the measured response at one or two observation points had to be satisfied. The general approach is a problem of constrained maximization of a forward solution, which is based on the Cauchy integral formula. The inclusion of an ocean into Weidelt's approach results in an additional constraint, because the observation points then become

fixed relative to the edge of a perfectly conducting half plane. Nevertheless, if the response at only one observation point is to be satisfied, the solution is straightforward. It leads to a system of equations that must be solved numerically, and which provides an upper limit for the depth of the top of an earth conductor near an ocean.

Acknowledgements. This work was funded by a University of Toronto Open Fellowship. Special thanks are due to K. Khan for drafting the figures and to S. Holladay and J. Macnae for providing plotting routines.

References

Bailey, R.C.: Electromagnetic induction over the edge of a perfectly conducting ocean: the *H*-polarization case. Geophys. J. R. Astron. Soc. **48**, 385-392, 1977

Bailey, R.C., Edwards, R.N., Garland, G.D., Kurtz, R., Pitcher, D.: Electrical conductivity studies over a tectonically active area in eastern Canada. J. Geomagn. Geolelectr. **26**, 125-146, 1974

Dawson, T.W., Weaver, J.T.: Three-dimensional induction in a non-uniform thin sheet at the surface of a uniformly conducting earth. Geophys. J. R. Astron. Soc. **59**, 445-462, 1979

Dosso, H.W.: A review of analogue model studies of the coast effect. Phys. Earth Planet. Inter. **7**, 294-302, 1973

Edwards, R.N., Greenhouse, J.P.: Geomagnetic variations in the eastern United States: evidence for a highly conducting lower crust? Science **188**, 726-728, 1975

Everett, J.E., Hyndman, R.D.: Geomagnetic variations and electrical conductivity structure in south-western Australia. Phys. Earth Planet. Inter. **1**, 24-34, 1967

Greenhouse, J.P., Parker, R.L., White, A.: Modelling geomagnetic variations in or near an ocean using a generalized image technique Geophys. J. R. Astron. Soc. **32**, 325-338, 1973

Honkura, Y.: Electrical conductivity anomalies in the earth. Geophys. Surv. **3**, 225-253, 1978

Hyndman, R.D., Hyndman, D.W.: Water saturation and high electrical conductivity in the lower continental crust. Earth Planet. Sci. Lett. **4**, 427-432, 1968

Koppenfels, W.v., Stallmann, F.: Praxis der konformen Abbildung. Grundlehren Math. Wiss., Vol. 100. Berlin: Springer 1959

Lilley, F.E.M., Woods, D.V., Sloane, M.N: Electrical conductivity from Australian magnetometer arrays using spatial gradient data. Phys. Earth Planet. Inter **25**, 202-209, 1981

Lines, L.R., Ainslie, B.A., Jones, F.W.: Investigation of the coastal effect by three numerical models. J. Geomagn. Geoelectr. **25**, 63-73, 1973

Morse, P.M., Feshbach, H.: Methods of theoretical physics, 2 vols. New York: McGraw-Hill 1953

Parkinson, W.D.: Directions of rapid geomagnetic fluctuations. Geophys. J. R. Astron. Soc. **2**, 1-14, 1959

Price, A.T.: A note on the interpretation of magnetic variations and magnetotelluric data. J. Geomagn. Geoelectr **15**, 241-248, 1964

Rikitake, T.: Electromagnetism and the earth's interior. Amsterdam: Elsevier 1966

Schmucker, U.: Anomalies of geomagnetic variations in the southwestern United States. J. Geomagn. Geoelectr. **15**, 193-221, 1964

Schmucker, U.: Anomalies of geomagnetic variations in the southwestern United States. Bull. Scripps. Inst. Oceanogr. **13**, 1-165, 1970a

Schmucker, U.: An introduction to induction anomalies. J. Geomagn. Geoelectr. **22**, 9-33, 1970b

Schmucker, U., Forbush, S.E., Hartmann, O., Giesecke, A A. jr., Casaverde, M., Castillo, J., Salgueiro, R., del Pozo, S.: Electrical conductivity anomaly under the Andes Carnegie Inst. Washington Yearbook **65**, 11-28, 1966

Vasseur, G., Weidelt, P.: Bimodal electromagnetic induction in non-uniform thin sheets with application to the northern Pyrenean induction anomaly. Geophys. J. R. Astron. Soc. **51**, 669-690, 1977

Weidelt, P.: The inverse problem of geomagnetic induction. Z. Geophys. **38**, 257-289, 1972

Weidelt, P.: Extremal models for electromagnetic induction in two-dimensional perfect conductors. J. Geophys. **49**, 217-225, 1981

Wolf, D.: Inductive coupling between idealized conductors and its significance for the geomagnetic coast effect M Sc thesis, Univ. Toronto, 1982a

Wolf, D: Comment on "Geomagnetic depth sounding by induction arrow representation: A review" by G.P Gregori and L.J. Lanzerotti. Rev Geophys. Space Phys **20**, 519-521, 1982b

Received July 6, 1982, Revised October 6, 1982;
Accepted November 2, 1982